Journal of Statistical Physics, Vol. 82, Nos. 5/6, 1996

Two-Dimensional Gas of Disks: Thermal Conductivity

Dino Risso[1] and Patricio Cordero[2]

Received February 2, 1995; final August 3, 1995

The phenomenon of heat conduction in a two-dimensional gas of N hard disks is studied in the hydrostatic regime by means of nonequilibrium molecular dynamics (N ranging from 100 to 8000). For systems with $N \geqslant 1500$ the temperature and density profiles observed are in excellent agreement with the continuous theory, but the conductivity k differs from the one derived from Enskog's theory in a systematic way. This difference seems to slowly decrease with increasing density.

KEY WORDS: Kinetic theory; thermal conductivity; molecular dynamics; hard disks; Enskog's Theory.

1. INTRODUCTION

Enskog's theory for transport coefficients arises from extending the Boltzmann formalism by introducing corrections that account for the fact that the molecular diameter is no longer small compared with the mean free path. A major consequence of this is that a mechanism of momentum and energy transfer which is negligible at lower densities becomes important, namely the collisional transfer of flux can be as important as the kinetic transfer. Still, Enskog's theory takes into account the correlations in position in an approximate way and does not consider correlations in velocity. In spite of these restrictions, Enskog's theory—which was developed for the case of bare hard spheres—is the best systematic description that yields transport coefficients in the context of kinetic theory.[1] Gass applied it to the case of hard disk.[2]

To test the validity of kinetic theory there is perhaps no better ground than computational simulations of many particle systems. In fact, one of

[1] Departamento de Física, Universidad del Bío Bío, Concepción, Chile.
[2] Departamento de Física, Universidad de Chile, Santiago, Chile.

0022-4715/96/0300-1453$09.50/0

the reasons why molecular dynamics (MD) simulations have the importance they have is that they provide essentially exact "experimental" data on well defined models. As there is no uncertainty about the form of the particle–particle and particle–wall interactions, theoretical predictions can be tested unambiguously in a manner that is generally impossible with data obtained in experiments with real fluids.

The first determinations of transport coefficients by means of *equilibrium* MD are found in ref. 3 (see also ref. 4). Later *nonequilibrium* MD was widely used. In ref. 5—studying a system of Lennard–Jones particles in the stationary regime under conditions that correspond to liquid argon—they were able to show that the Fourier law remains valid even for temperature gradients as big as 10^9 K/cm (see also ref. 6). In the case of a two-dimensional system of hard disks there is an extensive study of the decay of autocorrelation functions by equilibrium MD in ref. 7. In refs. 8 and 9 hard-disks nonequilibrium MD was applied to study space correlations in the presence of thermal gradients and thermal conductivity.

In this paper we have carefully studied the behavior of the conductivity k

$$k(\rho, T) = k_0(\rho)\sqrt{T} \tag{1.1}$$

of a two-dimensional system of N hard disks enclosed in a rectangular $L_X \times L_Z$ box, by means of nonequilibrium molecular dynamics. We pay particular attention to one value of the density ρ and explore the behavior of $k_0(\rho)$ for a few other values of ρ. Because the system has no intrinsic energy scale the temperature dependence of k can only be $\sqrt{T}$ if the Fourier law is true.

We know of no previous systematic study of the conductivity for this simple system using nonequilibrium MD. Since the cost of simulating it is possibly smaller than for any other interesting system (as explained in the next paragraph), a wider variety of situations can be explored to test kinetic theory using standard and common computational equipment.

As has been discussed in detail in the literature, the evolution of hard spheres (in 2D or 3D) can be efficiently simulated, because one goes from one collision to the next analytically.[10–12] There is no need to predefine a small time step in the program as necessary when continuous potentials are used. The time intervals by which the simulation proceeds are dictated by the dynamics itself. A comparison of the two cases (step versus continuous potentials) can be found in ref. 13, §II.D.

The transport coefficients of a system of hard disks are necessary also to analyze in depth many recent simulational results such as, for example, Bénard convection with hard-disk systems.[14–16] In fact, this paper is the

first of three dealing with the same system. The next two will be on viscosity and on Bénard convection.

In our simulations we can measure the local heat flux anywhere in the system and we can even separate the collisional from the translational contributions. Determining the conductivity in this way, however, is lengthy and noisy. We have preferred to measure the net heat flux Q_Z across the system as would be done in real experiments and define an *effective conductivity* k_{eff} which is the result of the different conductivities that the layers of this stratified system have.

An important technical detail comes from a known temperature jump that occurs at the walls when the system is subjected to a temperature difference ΔT. Because of this jump it is necessary to correct the temperatures at the walls by defining a new difference ΔT^*.

In Section 2 the characterization of the system, basic notation and the formal definition of the effective conductivity are given. Section 3 describes the way measurements are performed, the control parameters, the length of the simulations, and the basic physical characteristics of the dynamics of the system: equation of state and wall effects. In particular the already mentioned corrected temperature difference ΔT^* is defined here. The results are in Section 4: (a) Profiles of temperature and density obtained from the hydrostatic equations including Fourier's law show excellent agreement with the profiles obtained in the simulations. (b) The measurement of the net heat flux across the system and the use of the Fourier law yields an effective value for the effective conductivity k_{sim} for several values of the density. These values are compared with the effective conductivity that can be derived from Enskog's theory k_{theo} for the same densities. We find that the difference between the two conductivities (theoretical—coming from the approximations in Enskog's theory—and simulational) seems to decrease with increasing density.

Compare this situation with what happens for systems of hard spheres in 3D, where the differences increase with the density, as can be seen, for example, in ref. 3, where the authors studied a system of 108 hard spheres occupying a fraction of the total volume in the range from 0 to 0.52.

2. THE SYSTEM AND ITS HEAT CONDUCTIVITY

2.1. The System

The basic parameters of our system of hard disks are: the number of disks N; their mass and diameter m, D; the size of the rectangular box (L_X, L_Z); the acceleration of gravity g; and the temperatures at the top and

bottom walls $T_t = T_b - \Delta T$, T_b. The reduced temperature to which the system is subjected

$$C_t \equiv \frac{\Delta T}{T_b} \tag{2.1}$$

We define the aspect ratio $\lambda = L_X/L_Z$ and the *bulk area density* $\bar{\rho}_A = (\pi/4)\, ND^2/L_X L_Z$. In this way the lengths L_Z/D of the systems with different bulk densities are determined once we fix the number of particles N and the aspect ratio λ.

A system of hard disks locally obeys an equation of state that we take to be that of Henderson[18]

$$pL_X L_Z = NHk_B T, \qquad H(\rho_A) = \frac{1 + \rho_A^2/8}{(1-\rho_A)^2} \tag{2.2}$$

where $\rho_A = \rho_A(\mathbf{r}, t)$ is the local area density.

Because the system consists of only a few thousand particles, we need to use large temperature differences to have a good signal-to-noise ratio. Due to the important compressibility of this gas a significant density gradient would appear had we not added a linear external field (acceleration of gravity g) in the direction of the temperature gradient. Care has been taken to be outside the convective regime.[17] In most simulations g was in fact adjusted to produce a density profile as independent of height as possible. It can be shown[14] that if ΔT is relatively small, this happens when $Fr \approx H(\bar{\rho}_A)$ where Fr is defined by

$$Fr \equiv \frac{mgL_Z}{k_B \Delta T} \tag{2.3}$$

[Parenthetically we remark that the region of convection cannot be given in any simple way. For incompressible fluids the Rayleigh number Ra alone determines the zone in the control parameter space where there is convection, but in a forthcoming paper we will quantify the limiting line between the convective from the purely conductive zones in the Fr–Ra plane, which is not at all trivial. Besides, Ra is defined in terms of the conductivity (which we are studying in the present paper) and the viscosity, which will be studied next.]

The disks have elastic collisions among themselves. The vertical walls of the rectangular box are perfectly elastic, while the upper and lower walls simulate contact with heat baths at temperatures T_b at the bottom and T_t at the top. It would have been simpler to use periodic vertical conditions instead of elastic walls, but the runs used in the present study are an

inseparable unit from those that study the convective regime. In our conventions a disk hits a wall when its center does so. When a particle hits a horizontal wall the tangential component is conserved while the normal component is sorted from the Maxwellian distribution associated with the temperature of the wall (stress free boundary conditions).

A set of values for ΔT is used to be able to extrapolate to $\Delta T = 0$. Further since the system is finite we have to see the behavior of the conductivity as a function of the number of particles and in this way be able to see the tendency as N goes to infinity. Our results in this respect are in fig. 4 and we are unable to draw a clear conclusion. For three values of N (900, 1521, and 8100) we have enough statistics and there is a slight increase of k with N.

2.2. Heat Flux and Effective Conductivity

From Q_z one can define the *effective conductivity* of the system as

$$k_{\text{sim}} = \frac{Q_Z L_Z}{\Delta T} \tag{2.4}$$

Since the system has an important temperature gradient we directly compare the effective conductivity obtained by means of the simulations using (2.4) with the effective conductivity k_{theo} that stems from Enskog's theory.

2.3. Theoretical Effective Conductivity

The expression for the conductivity k for a gas of hard disks predicted by Enskog's theory has the form (1.1) and is given by

$$k = 1.029 \frac{2k_B}{D\chi(\rho_A)} \left(\frac{k_B T}{m\pi}\right)^{1/2} \left[1 + \frac{3}{2}(2\rho_A \chi(\rho_A)) + 0.8718(2\rho_A \chi(\rho_A))^2\right] \tag{2.5}$$

where χ is the pair correlation function at contact[27]

$$\chi(\rho_A) = \frac{H-1}{2\rho_A} = \frac{1-(7/16)\rho_A}{(1-\rho_A)^2} \tag{2.6}$$

Since (2.5) depends on the local values of the density and temperature, we define, in a straightforward manner, a *theoretical effective conductivity* k_{theo} for the system as a whole as the limit $\delta \to 0$ of

$$k_{\text{theo}} = \left(\frac{1}{N_{\text{slices}}} \sum_{i=1}^{N_{\text{slices}}} k_i^{-1}\right)^{-1} \tag{2.7}$$

where each i represents a horizontal slice of width δ of the system. For our purposes, however, we have used (2.7), evaluating a set of $k_i(\rho_A, T)$ from (2.5) using the observed average values of ρ_A and T, averaged in each horizontal slice i. The logic behind (2.7) is the same as used to obtain the effective resistance ($r = 1/k$) of a system of resistors (the horizontal slices) connected in series. Although it is easy to derive, it is better to simply think of the parallel between $\mathbf{q} = -k\,\nabla T$ and $\mathbf{J} = -g\,\nabla V$, where J is the electric current density, V is the electric potential, and g the electric conductivity).

3. OBSERVATION MEANS AND METHODS

3.1. Observation Cells

To make the observations we have made use of our own efficient algorithm[12] and the carefully devised measurement routines described in ref. 17. The system is divided in *cells* to observe its behavior. The routines make a detailed balance of the mass, momentum, and energy in each cell (these are densities) and what comes in or out across each of the walls of every cell (fluxes). The measured quantities are then averaged in time in every cell or wall depending on whether they are densities or fluxes. At the end we have mainly used horizontal averages of the observed quantities, leaving out the observations near the vertical and horizontal walls. A *standard observation mesh* was chosen depending on N and the area density $\bar{\rho}_A$. In most simulations we used a cell mesh of 15×15.

3.2. Control Parameters

In principle the set of possible control parameters is rather large: g, $\Delta T = T_b - T_t$, the bulk area density $\bar{\rho}_A$, N and $\lambda = L_X/L_Z$. We considered systems with N ranging from 100 to 8000 inside a box of aspect ratio $\lambda = 1$. In most of the simulations the density was chosen as $\bar{\rho}_A = 0.2$ and $N = 1521$, while Fr and C_t were used as control parameters.

The regime in which the density profile is flatter [$Fr \approx H(\rho_A)$] is easier to analyze since in this case the density variation effects—to determine k as a function of the local values ρ_A of the area density—are smaller.

3.3. Simulation Times

To determine the length of the simulations we considered the thermal diffusion time $t_{\text{diff}} \sim L_Z^2/\kappa$ measured in number of collisions (where κ is the thermal diffusivity). During this time the number of collisions $N_{\text{diff}}^{\text{col}}$ is Γt_{diff},

where Γ is the total collision rate. From Enskog's theory applied to a gas of N hard disks it is known that the total collision rate is[2]

$$\Gamma = \frac{4\rho_A N \chi(\rho_A)}{D(k_B T/\pi m)^{1/2}} \tag{3.1}$$

The characteristic time for the thermal diffusivity is $t_{\text{diff}} = L_Z^2/\kappa = \gamma k_B N/\lambda k$, where $\gamma = \gamma(\rho_A) = c_p/c_v \approx 2$. Using (2.5) and (3.1) we obtain the number of collisions in one t_{diff}:

$$N_{\text{diff}}^{\text{col}} = \gamma \frac{N^2}{\lambda} \frac{2\rho_A \chi^2}{1.029[1 + (3/2)(2\rho_A \chi(\rho_A)) + 0.8718(2\rho_A \chi(\rho_A))^2]} \tag{3.2}$$

Hence $N_{\text{diff}}^{\text{col}} \sim 4\rho_A N^2$, which corresponds to an average of $8\rho_A N$ collisions per disk in one diffusion time. In every run there was a thermalization period, typically of $10t_{\text{diff}}$ (which means about 24,000 disk–disk collisions per disk in the case of a system of $N = 1521$ particles and a density of $\rho_A = 0.20$), after which time averages were taken during the last 10–40 diffusion times (initially the particles are placed regularly with velocities sorted from Maxwellian distributions with T varying linearly from T_t to T_b according to height).

3.4. Local Equation of State

Having subjected our system to large temperature differences and with large values for g the equilibrium equation of state is observed to be valid

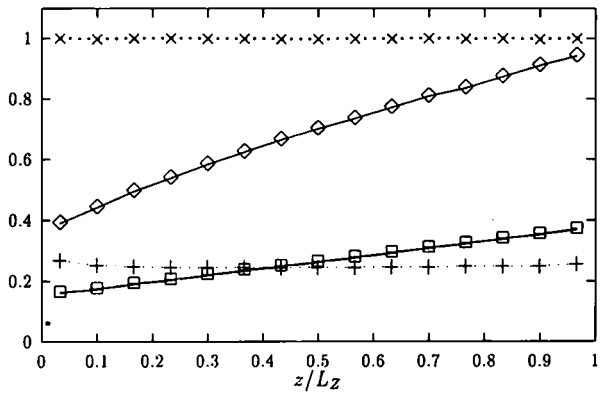

Fig. 1. Profiles of pressure (□), density (+), and temperature (◇) versus height z for a system with $N = 1521$, $\bar{\rho}_A = 0.2$, $Fr = 1.56$, and $C_t = 0.624$. The ratio $pL_X L_Z/NHk_B T$ (×) is also plotted.

in the range $Fr = 0.3$–1.7 with C_t up to its maximum value $C_t = 1$. This is true even when there is convection.[17] In Fig. 1 we show typical vertical density, pressure and temperature profiles obtained for a system of 1521 particles with $\bar{\rho}_A = 0.2$ and $C_t = 0.624$. The figure also shows how well the equation of state is satisfied, plotting the ratio $I \equiv pL_X L_Z / NH(\rho_A) k_B T$ using the values of p, T, and ρ_A obtained from the simulation. The observed values of the ratio I differ by less that 1% from unity when Henderson's equation of state (2.2) is used.

3.5. Wall Effects at Equilibrium

An important effect in simulations with a few thousand particles is the magnitude of the boundary effects of microscopic origin. To be able to quantify these effects we first made simulations in thermal equilibrium with and without gravity.

One well-known effect is the density peak near hard walls.[19–21] For a system of 1521 disks the density was measured in an exceptionally fine mesh of 77×77. The density was observed to go up about 15% for a system with a bulk density of $\bar{\rho}_A = 0.2$. The width of this denser boundary layer is about one free path. In our case the wall effects were negligible beyond the first standard observation cell. Had we chosen higher densities, the boundary effects would be larger, but not wider. No boundary effect for the temperature (at equilibrium) was observed.

3.6. Wall Temperature Jump

Once a conductive regime is established, the measured temperature difference in the bulk is smaller than the externally imposed difference. This is a well-known effect[5, 22] due to a temperature discontinuity at the walls. A similar effect is observed in real, dilute systems.[23] This temperature discontinuity is related to both the collision rate and the temperature difference. In fact, the discontinuity of $T(\mathbf{r})$ near hard walls is an effect of the stochastic thermalization at the walls. A simple derivation of it is the following. The relation between the externally imposed temperature difference and the measured temperature difference can be estimated assuming local thermodynamic equilibrium and taking into account the rate of energy interchange in collisions with the thermalizing walls. Calling T_b^* and T_t^* the temperatures near the lower and upper walls *inside the fluid*, the flux of energy across the walls can be written as $Q_b = \frac{3}{2} \Gamma_b k_B (T_b - T_b^*)$ and $Q_t = \frac{3}{2} \Gamma_t k_B (T_t^* - T_t)$, where $\Gamma_j (j = b, t)$ are the disk–wall collision rates at the two thermalizing walls. The factor 3/2 comes from the velocity distribution of the particles hitting the wall. In the stationary case it is necessary

(Fourier law) to have that $Q_b = Q_t = k_{\text{eff}}(T_b^* - T_t^*)/L_Z$ and from this, if the imposed temperature difference is ΔT, the effective difference ΔT^* is

$$\Delta T^* = (1+\varepsilon)^{-1}\,\Delta T \tag{3.3}$$

where

$$\varepsilon \equiv \frac{2}{3}\left(\frac{1}{\Gamma_b}+\frac{1}{\Gamma_t}\right)\frac{k_{\text{eff}}}{k_B L_Z}$$

depends on the particle–wall collision rates Γ_b and Γ_t at the lower and upper walls, respectively.

Notice that the number of particles enters this expression through the height L_Z of the system as $L_Z = (\pi N/4\rho_A\lambda)^{1/2}D$. Keeping λ and $\bar{\rho}_A$ fixed, L_Z diverges as $\sqrt{N}$, making ε vanish in the large-N limit. For a system of $N = 1521$ particles, $\bar{\rho}_A = 0.2$, $C_t = 0.5$, and $L_Z = 78D$ we get $\Delta T^*/\Delta T \approx 0.85$, which approximately corresponds to the temperature jump ratio observed in our simulations.

Extrapolating the observed temperature profile from the bulk, the simulations yield the effective temperatures at the walls and from here we get the effective temperature difference ΔT^* (and also the effective temperature ratio $C_t^* \equiv \Delta T^*/T_b^*$ and $Fr^* = mgL_Z/k_B\Delta T^*$) which will be used in (2.4) to make comparisons with the conductivity predicted by Enskog's theory.

4. OBSERVATIONS AND COMPARISONS WITH THE THEORY

4.1. Density, Temperature, and Pressure Profiles

Numerically solving the NS equations under hydrostatic conditions making use of (a) Henderson's equation of state (2.2), (b) Fourier's law, (c) the conductivity $k(\rho_A(z), T(z))$ taken from Enskog's theory, (d) the effective temperature values T_t^*, T_b^* and (e) the condition that $\bar{\rho}_A L_Z = \int \rho_A(z)\,dz$, it is possible to find the theoretical density, temperature, and pressure profiles. In Fig. 2 we compare these profiles with those obtained from the simulations for typical values of the imposed Fr and C_t. Excellent agreement is obtained. We remark that these comparisons are made not only when ρ_A is approximately constant [$Fr^* \equiv mgL_Z/(k_B\Delta T^*) \approx H(\bar{\rho}_A)$], but also when the density varies significantly with height. In the comparison with theoretical results (below), we make some remarks regarding this agreement. Note that near the borders ($z = 0$ and $z = L_Z$) the density profile is distorted by boundary effects.

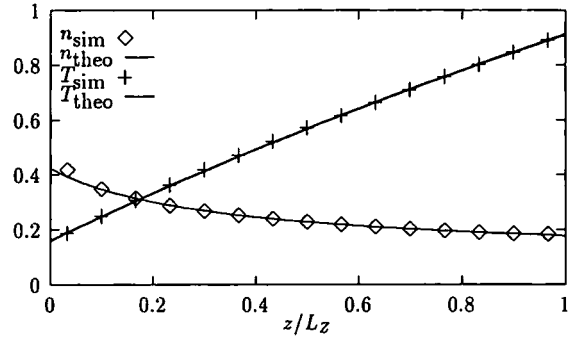

Fig. 2. Density and temperature profiles obtained from our simulations and from the theory for $N = 1521$, $\bar{\rho}_A = 0.20$, $C_t^* = 0.786$, $Fr^* = 0.379$.

4.2. The Effective Conductivity k

Figure 3 shows a comparison of the values of k versus C_t^* obtained from the simulations with $N = 1521$, $\bar{\rho}_A = 0.2$, and $Fr^* \approx 1.56$ using (2.4) with the theoretical conductivity, (2.7). To get the results summerized in Fig. 3 we used seven different simulations for each C_t, starting from initial conditions that are microscopically different but macroscopically equivalent (same density and velocity profiles). Note that because of the statistical fluctuations in the measured values of T_t^* and T_b^* the values of C_t^* show a dispersion for every externally imposed C_t. For $C_t^* < 0.3$ only one

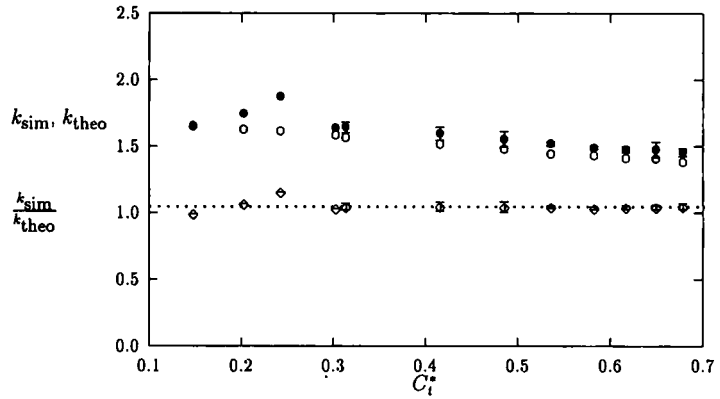

Fig. 3. Conductivities k_{sim} (•) and k_{theo} (∘) and their ratio (◇) versus C_t^* for a system with $N = 1521$, $\bar{\rho} = 0.20$, $Fr^* = 1.56$. The dotted line indicates the mean value 1.044 of the ratio.

simulation was made for every C_l. The observed values of k are systematically larger than the theoretical values.

For a remarkably wide range of values of C_l^* the ratio $k_{\text{sim}}/k_{\text{theo}}$ is nearly constant (Fig. 3) in spite of the large temperature variations across the system. This can be understood from (2.7)—assuming that the density is about uniform (and equal to $\bar{\rho}_A$)—because one can then derive that $k_{\text{eff}} \approx k_0(\bar{\rho}_A)L_Z/\int dz/[T(z)]^{1/2}$. To evaluate the ratio $k_{\text{sim}}/k_{\text{theo}}$ the same temperature profile is used in the numerator and denominator and therefore this factor cancels out. Only the ratio between the k_0's remains.

For the case $\bar{\rho}_A = 0.2$, $Fr^* = 1.56$, and $N = 1521$ (leaving out cases for which the signal/noise ratio is too small, i.e., $C_l^* < 0.5$), the extrapolation from these simulational results yields $k_{\text{sim}}/k_{\text{theo}} = 1.044 \pm 0.004$.

4.3. Comparison with Theoretical Profiles

We would like to understand why the observed profiles fit so well the theoretical predictions (as in Fig. 2) while the observed conductivity shows an indisputable difference from Enskog's prediction. In other words, how is it possible to have a discrepancy in the conductivity without having one in the profiles?

From a theoretical point of view we know that k has the form (1.1) and any correction can be written as a corrective factor $C(\rho_A)$ affecting the particular k_0 given in (2.5).

First let us notice that the local conductivity enters the formalism only through the energy balance equation, which in hydrostatics simply is $\nabla \cdot \mathbf{q} = 0$, namely, $\nabla \cdot (k \nabla T) = 0$. Since the only coordinate that matters is z, the last equation is $(kT')' = 0$ or $T''/T' = -k'/k$. If we use (1.1), $k = k_0\sqrt{T}$, then the T-profile equation is

$$T''/T' + T'/(2T) = k_0'/k_0 = (k_0^{-1}\, dk_0/d\rho_A)\rho_A'$$

Making the change $k_0 \to Ck_0$ in the last expression amounts to changing $k_0^{-1}\, dk_0/d\rho_A$ by $k_0^{-1} dk_0/d\rho_A + C^{-1} dC/d\rho_A$, adding a term $C^{-1} dC/d\rho_A$ on the right-hand side. From the factor k_0 in (2.5) one can get that $k_0^{-1}\, dk_0/d\rho_A$ grows smoothly from 3.44 at $\rho_A = 0.15$ to 9.0 at $\rho_A = 0.55$, while from the data summarized in Fig. 5 one can estimate that about $\rho_A = 0.2$ that value of $C^{-1} dC/d\rho_A$ is about 0.013. Namely, the observed correction to the conductivity would affect the temperature and density profiles by less than 0.3%.

4.4. On size effects

Figure 4 shows the ratio $k_{\text{theo}}/k_{\text{sim}}$ for $N = 100$, 300, 900, 1521, 2500, and 8100. For $N = 100$, 300 and 2500 only one initial condition was taken

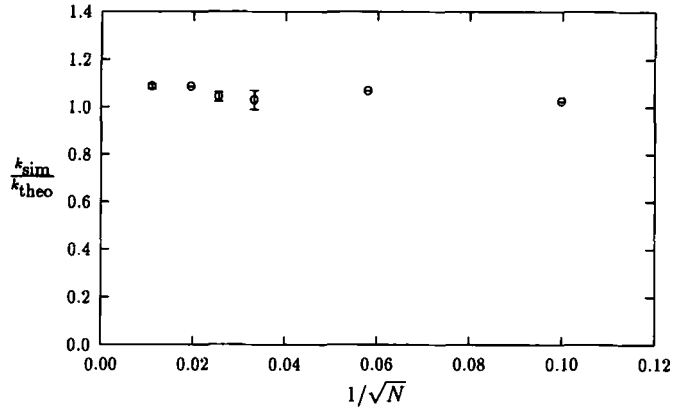

Fig. 4. Ratio k_{sim}/k_{theo} versus $1/\sqrt{N}$.

while C_t was changed (hence no error bars in these cases). For $N=8100$ only two initial conditions were considered, while for $N=900$ and 1521 seven different initial conditions were considered. The cases $N=900$, 1521, and 8100 indicate that the ratio is slightly increasing with N, but for the excessive computational cost we disregarded the possibility of making more simulations with $N=$ 8100 or simulations with larger N. We draw no conclusions.

4.5. Other Values for the Density

Though we have not made a systematic study of the conductivity as a function of the density we obtained the ratio k_{sim}/k_{theo} for different densities ($\bar{\rho}_A=0.1$, 0.2, 0.3, 0.4 and 0.5) in the case of a system of $N=1521$ particles with $Fr^*=H(\bar{\rho}_A)$. These ratios are plotted in Fig. 5.

We see that the most important discrepancies with Enskog's predictions seem to take place for $\rho_A \approx 0.2$. This may seem strange since one should think that the discrepancies increase with the density. But from our results it seems that the higher order corrections that come in beyond Enskog's theory go down with the density, eventually changing sign. To support this, we have the above results and a recent one[26] where the authors show that for a system of particles at $\bar{\rho}_A=0.55$—interacting with a hard (but not infinitely hard) potential—the ratio of conductivities is 0.93. This result, seen in Fig. 5 as an open circle, roughly follows the tendency of our results.

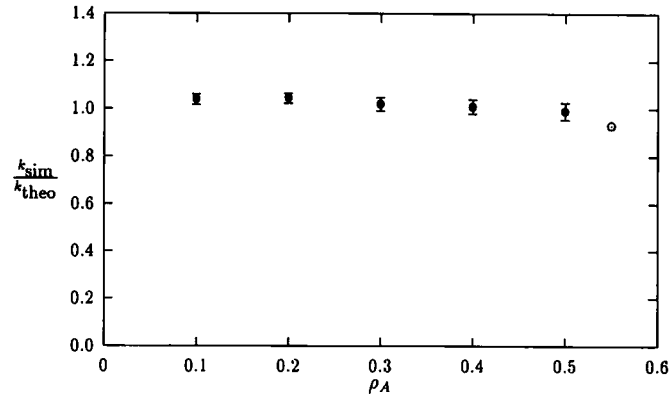

Fig. 5. Observed values for the ratio k_{sim}/k_{theo} versus $\bar{\rho}_A$ for systems of $N = 1521$ particles. The open circle is the ratio reported in ref. 26 (see text).

FINAL COMMENTS

1. In this paper we assumed that the Fourier law is valid. We were able to obtain excellent agreement between theory and simulations regarding the density and temperature profiles when the bulk density is $\bar{\rho}_A = 0.2$.

2. Next, we were able to define an effective conductivity in such a way that the ratio k_{sim}/k_{theo} is independent of the temperature difference for a wide range of density values ($\bar{\rho}_A$ from 0.1 to 0.5). This independence from the temperature difference validates Fourier's law for our system and allows us to extrapolate the value of the conductivity to the limiting case $\Delta T = 0$ for different values of the density $\bar{\rho}_A$.

3. The ratio k_{sim}/k_{theo} however, unequivocally differs from unity. For intermediate densities ($\bar{\rho}_A$ about 0.2) the effective conductivity is larger than the one predicted by the theory while it starts to go down for larger values of $\bar{\rho}_A$ and finally the simulational conductivity appears to be slightly smaller than the theoretical value when $\bar{\rho}_A \approx 0.5$.

4. To understand why it is consistent that the profiles (item 1 above) fit so well while the conductivity does not (item 3), we observed that the corrective factor $C(\rho_A)$ multiplying the Enskog's k_{theo} is so weakly dependent on density—for the case $\bar{\rho}_A = 0.2$—that it cannot be detected in the density and temperature profiles.

ACKNOWLEDGMENTS

The work of D. R. was partially financed by the Universidad del Bío Bío research grand DIPRODE 941705-1. The work of P.C. was partially financed by the Fondecyt research grant 193-1105.

REFERENCES

1. J. H. Ferziger and H. G. Kaper, *Mathematical Theory of Transport Processes in Gases*, (North-Holland, Amsterdam, 1972).
2. D. Gass, *J. Chem. Phys.* **54**:1898 (1971).
3. B. J. Alder and T. E. Wainwright, *Phys. Rev. A* **1**:18 (1970).
4. D. Levesque, L. Verlet, and J. Kürkijarvi, *Phys. Rev. A* **7**:1690 (1993).
5. A. Tenenbaum, G. Ciccotti, and R. Gallico, *Phys. Rev. A* **25**:2778 (1982).
6. G. Ciccotti, In *Microscopic Simulations of Complex Flows*, M. Marechal, ed. (Plenum Press, New York, 1990).
7. J. J. Erpenbeck and W. W. Wood, *Phys. Rev. A* **26**:1648 (1982).
8. M. Mareschal and E. Kestemont, *Phys. Rev. A* **30**:1158 (1984).
9. M . Mareschal, In *Molecular Dynamics Simulations of Statistical-Mechanical Systems*, G. Ciccotti and W. G. Hoover, eds. (North-Holland, Amsterdam 1986), p. 325.
10. D. C. Rapaport, *J. Comp. Phys.* **34**:184 (1980).
11. B. D. Lubachevsky, *J. Comp. Phys* **94**:225 (1991).
12. M. Marin, D. Risso, and P. Cordero, *J. of Comp. Phys.* **109**:306 (1993).
13. D. C. Rapaport, *Phys. Rev. A* **46**:1971 (1992).
14. M. Mareschal and E. Kestemont, *J. Stat. Phys.* **48**:1187 (1987); A. Puhl, M. Malek-Mansour, and M. Mareschal, *Phys. Rev. A* **40**:1999 (1989).
15. D. C. Rapaport, *Phys. Rev. Lett.*, **60**:2480 (1988), D. C. Rapaport, *Phys. Rev. A* **46**:1971 (1992).
16. D. Risso and P. Cordero, In *Condensed Matter Theories*, A. N. Proto and J. Aliaga, eds. (Plenum Press, New York, 1992); D. Risso and P. Cordero, In *Proceedings of the IV Instabilities and Nonequilibrium Structures*, E. Tirapegui and W. Zeller, eds. (Kluwer, Dordrecht, 1992).
17. D. Risso, Ph.D. thesis, Universidad de Chile (1994).
18. D. Henderson, *Mol. Phys.* **30**:971 (1975).
19. F. F. Abraham, *Phys. Rep.* **53**:93 (1979).
20. M. P. Allen, and D. J. Tildesley, *Computer Simulation of Liquids* (Clarendon Press, Oxford, 1989).
21. J. P. Hansen and I. R. McDonald, *Theory of Simple Liquids*, 2nd ed. (Academic Press, New York, 1986).
22. C. Trozzi, and G. Ciccotti, *Phys. Rev. A.* **29**:916 (1984).
23. J. O. Hirschfelder, C. F. Curtiss, and R. B. Bird, *Molecular Theory of Gases and Liquids* (Wiley, New York, 1954).
24. W. G. Hoover, *Molecular Dynamics* (Springer-Verlag, New York, 1986), pp. 65, 130.
25. G. Ciccotti and W. G. Hoover, *Molecular Dynamics Simulations of Statistical-Mechanical Systems* (North-Holland, New York, 1986), comment by M. Mareschal, p. 325.
26. M. Mareschal and U. Krebs, In *Proceedings of the Eurotherm* 36 *Conference*, to appear.
27. J. A. Barker and D. Henderson, *Rev. Mod. Phys.* **48**:587 (1976).